Study of the flash ignition time of air plasma formed through laser-induced breakdown

GUIXIA WANG, JUNHONG SU*, JUNQI XU, QINGSONG WANG
The department of photoelectric engineering, Xi'an Technological University, Xi'an, 710021, China

The air and thin film plasma(AP and TFP) sparks may be generated at the same time when high-energy laser acts on the surface of the thin film. AP sparks and TFP sparks are often misjudged when the plasma sparks of laser-induced thin film damage is detected. Measuring the flash ignition time (referred to as "spark time" or "ST") of AP enables researchers to accurately distinguish AP and TFP sparks and eliminate film damage discrimination that occurs when using plasma flash methods. A Nd:YAG nanosecond-pulse laser with 1064 *nm* wavelength was employed to generate AP and AP sparks through induced-laser breakdown in air. The incident laser and AP spark signals were collected using high-speed free-space detectors and processed using an oscilloscope. These signals were computed and analyzed to obtain the ST of the AP sparks produced during laser-induced breakdown and observe the variations in ST with different laser intensities. Finally, the multiphoton absorption and cascade ionization theories were applied to calculate and compare theoretical STs to the experiment results. Findings showed that the experimental STs decreased slightly with an increase in laser intensity. Moreover, the experimental STs were extremely consistent with the theoretical STs, verifying the feasibility of the proposed experiment method.

(Received February 2, 2018; accepted August 9, 2018)

Keywords: Laser-induced breakdown, Air plasmas, Thin films, Plasma sparks

1. Introduction

In high-energy laser application systems, the continuous application of high-power lasers can break down air and optical films into plasma and ignite the plasma to form flashes (hereafter referred to as "sparks"). Previous studies indicated that multiphoton absorption (MPA), i.e., cascade ionization (CI), is the primary cause for air breakdown [1–9]. The development of air plasma (AP) can be characterized by four stages [10]. The first stage is the initialization stage wherein the incident laser irradiates a focal point to form initiating electrons. This is the beginning of spark development. The second stage is the plasma growth stage wherein CI causes the free electrons and ions in the air to multiply rapidly, consequently increasing the electron density at the focal point to a specific threshold (density that causes air breakdown). The third stage is the development and distribution of shock waves accompanying the AP in the focal plane. The fourth stage is the dissipation of the AP. The spark time (ST) of AP refers to the period from the irradiation of the laser on the focal point until a spark is produced. Therefore, ST can be defined as the time required to complete the first and second stages. Although AP sparks produced during laser-induced breakdown and the aforementioned four stages have been extensively studied by a number of scholars [10–20], few have analyzed the ST of AP produced during laser-induced breakdown. AP sparks and thin film plasma (TFP) sparks are often misjudged when detecting the plasma sparks of laser-induced thin film damage [21–22]. A number of scholars reported that when a laser is concentrated on the target material, the plasma ST of the target material and the ST of the AP are different [23–24]. Therefore, by determining the STs of AP and TFP produced during laser-induced breakdown, researchers can use the time differences to identify AP and TFP sparks accurately. In this study, an experiment was designed to measure the ST of AP produced during laser-induced breakdown. The results are then compared to the ST of AP obtained through theoretical computation to analyze the effects of incident laser power on ST. The findings obtained in this study not only revealed the mechanisms involved in the formation, growth, and expansion of AP during laser-induced breakdown but also provided a technical basis for detecting the plasma sparks of thin film damage, thereby fundamentally eliminating the discrimination of thin film damage that occurs when using the plasma flash method and providing new concepts for gas dynamics research concerning high-power laser-induced breakdown of air.

2. Numerical computation for the flash ignition time of air plasma

In atmospheric air, this transformation from neutral air into hot plasma occurs in three distinct stages: initiation, formative growth, and air plasma spark. A fourth and final stage, extinction, follows. The first stage refers to MPA, this process begins with the release of a free electron, and the growth in the free electron and ion

concentrations in the air. The second stage is formative growth stage under the action of CI, during which the number of free electrons and ions increases until the state of "breakdown" is reached. Air plasma spark time (t_b) can be defined as the time required to complete the first and second stages. Therefore, in order to obtain the air plasma spark time (t_b), the processes of MPA and CI will be analyzed above. In MPA, photo-excitation corresponds to the absorption of a photon as a result of which the atomic system is raised to a higher state. Photo-deexcitation is simply the converse emission process. Photo-ionization can occur when an incident photon has sufficient energy to remove an electron fiom an atomic system thus leaving it in a higher stage of ionization. In photo recombination the electron recombines with an ion with the emission of a photon. In this process, an atom simultaneously absorbs a k^{th} number of photons, where total k photons energy is greater than the atom's ionization potential. This absorption causes the atom to ionize. During the formation of AP, electron density (n_{e1}) changes over time (t).The equation can be expressed as follows [10,21]:

$$\frac{dn_{e1}}{dt} = \frac{AN}{k^{\frac{3}{2}}} I^k(\mathrm{t}) \tag{1}$$

where $I(\mathrm{t}) = I_0 \exp\{-4\ln 2[(\mathrm{t}-\tau_p)^2 / \tau_p{}^2]\}$ is the principle for the change of laser pulse over time, $I_0 = E/(\tau_p \pi r^2)$ is the initial intensity of the incident laser, $A = \sigma^k / [w^{k-1}(\mathrm{k}-1)!(\mathrm{h}\, w)^k]$ is the MPA rate, $w = 2\pi c/(\lambda n)$ is the optical frequency, τ_p is the pulse width, E is the energy of the incident laser, r is the radius of the focal point of the incident laser, N is the density of the air molecules, k is the number of photons that must be simultaneously absorbed to ionize an atom, σ is the photon absorption cross section of the atomic step, and $h = 6.626\times10^{-34}$ is the Planck constant.

Naturally formed electrons and early electrons created through multiphoton ionization are typically present in the laser irradiation area. These electrons are commonly referred to as initiating electrons. Initiating electrons are activated by the laser's electric field. With sufficient energy, atom excitation and ionization occur during collision. Continuous collision consequently causes electron collapse or CI. During CI, electron density (n_{e2}) changes over time (t). The equation can be expressed as follows [10,21]:

$$\frac{dn_{e2}}{dt} = n_{e2} N[\frac{377q}{w^2}(\frac{\nu_m}{N})^2] \cdot I(\mathrm{t}) \tag{2}$$

where q is the air coefficient, ν_m is the electron collision frequency for momentum transfer, $c = 3\times10^8 (m/s)$ is the speed of light, λ is the wavelength of the incident laser, and $n = 1.0003$ is the refractive index of air.

Equations (1) and (2) can be combined to calculate the electron density (n_e) of a specific gas over time (t) while taking MPA and CI into account. The merged equation can be expressed as follows:

$$\frac{dn_e}{dt} = \frac{dn_{e1}}{dt} + \frac{dn_{e2}}{dt} = n_{e2} N[\frac{377q}{w^2}(\frac{\nu_m}{N})^2] \cdot I(\mathrm{t}) + \frac{AN}{k^{\frac{3}{2}}} I^k(\mathrm{t}) \tag{3}$$

In Eq. (3), $N = 2.7\times10^{19}(cm^{-3})$, $q = 10^{21}(cm^{-1}s^{-1}\,\mathrm{V}^{-2})$, $\nu_m = 3.9477\times10^{13}(s^{-1})$, $\nu = 10^{15}(s^{-1})$, $\sigma = 10^{-16}(cm^{-2})$.

Under normal temperature and pressure, the moment of air breakdown can be defined as the moment corresponding to $n_e = 10^{13} cm^{-3}$. At this moment, air is broken down, and AP is ignited [10,21–22]. As shown in Equations (3), Laser wavelength, incident laser energy, pulse width, and laser facula radius are the main factors that affect the air plasma spark time t_b. If $\lambda = 1.064\times10^6$ (m), $\tau_p = 10^{-8}(s)$, and $r = 0.015(cm)$, the laser wavelength, pulse width, and laser facula radius are constants, then only the variation of air plasma spark time t_b with laser energy have been analyzed. The laser energy chosen have a requirement that must be greater than the energy threshold of air breakdown. The energy threshold of air breakdown is related to many factors, such as ambient temperature, humidity and laser action parameters. It is found that the energy threshold of the air is about 150mJ under the conditions of the experimental environment and the parameters of the laser in this paper, so the laser intensities of 160 mJ, 200 mJ, and 230.59 mJ, which is larger than 150 mJ, is randomly selected.

Using the equation (3), the t_b simulation results using different laser intensities are illustrated in Fig. 1.

Fig. 1 indicates that when other conditions are unchanged, the greater the laser energy, the easier the air will be broken down, and the less air plasma spark time t_b it will be. Under the same condition that other conditions are unchanged, from the microscopic point of view, the greater the incident laser energy, the greater the energy absorbed by the air. Then, the plasma with high temperature was generated earlier. The plasma absorbed the residual energy of the laser and expanded rapidly, forming a plasma flash. From a macroscopic point of view, the greater the incident laser energy, the shorter time it takes to ionize the same atom after the air absorbs energy. Therefore, air plasma spark time t_b decreases with increasing laser intensity E.

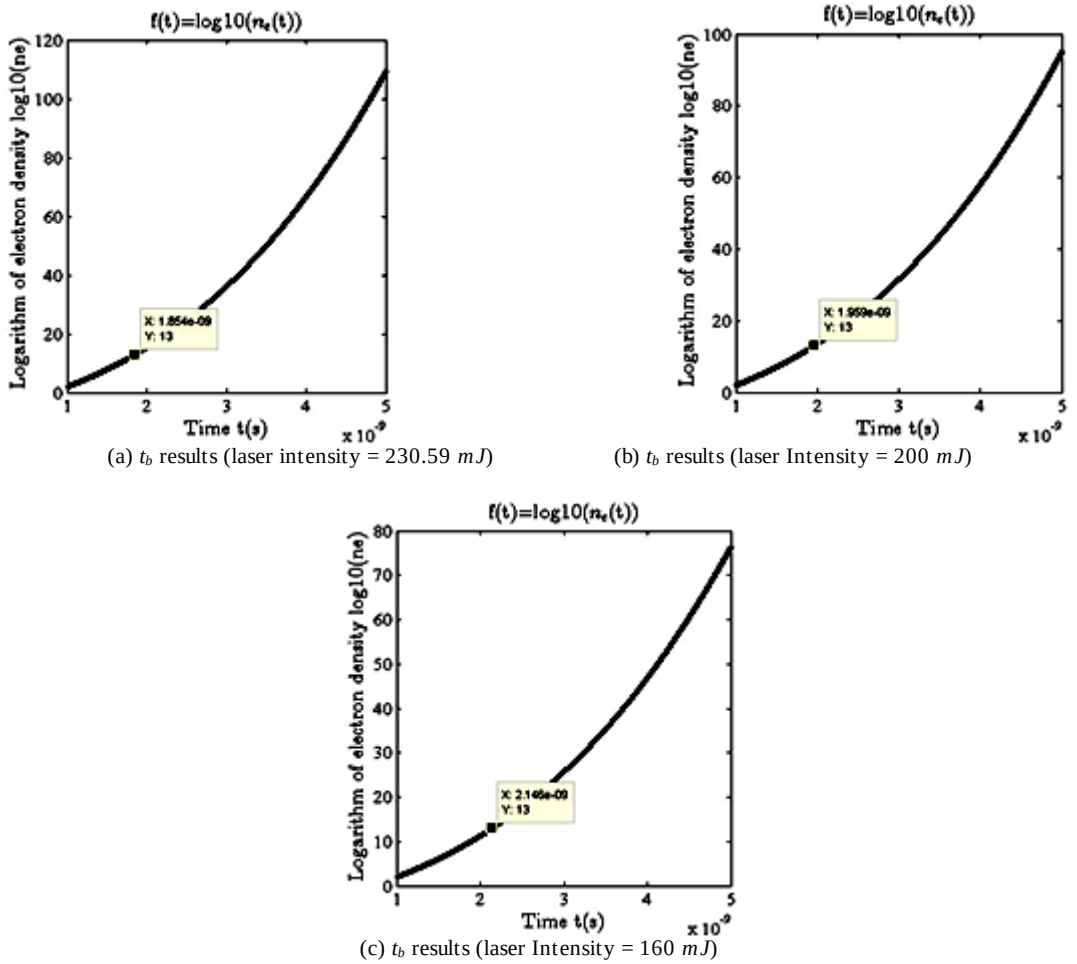

(a) t_b results (laser intensity = 230.59 *mJ*)

(b) t_b results (laser Intensity = 200 *mJ*)

(c) t_b results (laser Intensity = 160 *mJ*)

Fig. 1. t_b calculation results using different laser intensities

3. Experimental test system and configuration

A schematic representation of the AP sparks produced during laser-induced breakdown is illustrated in Fig. 2. In the figure, a high-power Nd:YAG laser (1) is passed through a filter (2) and an attenuator (3). A focusing system (4) concentrates the laser on the sample stage (7). The air surrounding the specimen breaks down and forms plasma sparks. An energy meter (6) promptly reads the reflected light energy released by the beam splitter (5). A computer (8) serves as the operation console. The two probes (9 and 10) are the high-speed free-space detectors, DET08CL/M and DET025AL/M, manufactured by THORLABS. Taking into account the speed of light, the signals collected by the detectors can be characterized as the moment at which the incident laser reaches the focal point and the moment at which a plasma spark begins. The light signals are converted into electric signals and compared. The difference between the two sets of signals is the ST of the AP produced during laser-induced breakdown (t_b). The two sets of electric signals are processed using the Tektronix MSO2024B four-channel oscilloscope (12) to produce a curve that shows the changes in signal voltage over time. The voltage occurrence of the two sets of signals corresponding to the time difference is t_b. To protect Probe 9 from the immense energy of the incident laser, a set of annuates (11) are placed between the laser and the probe.

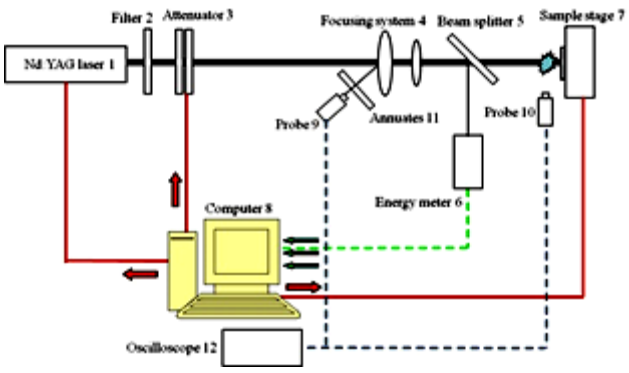

Fig. 2. Schematic of the experiment

The partial configuration of the experiment is illustrated in Fig. 3. The high-power Nd:YAG solid-state laser emits a wavelength of 1064 *nm*. The laser's output is

adjustable between 5 *mJ* and 235 *mJ*, the radius of the focal point is 0.015 *cm*, and the pulse width is 10 *ns*. For stability, the laser output is fixed at a specific voltage. The maximum bandwidths of Probe 9 and Probe 10 are 5 GHz and 2 GHz, respectively. Because the incident laser wavelength is 1064 *nm*, in order to collect the incident laser signal, it is necessary to use the near infrared photodetector, and the air plasma flash spectrum is mostly in the visible region, so the visible light detector is used to collect the air plasma flash. In this paper, the measurable spectra of the two probes are between 800 and 700 *nm* and 400 and 1100 *nm*, respectively. The surge times of the two probes are 70 *ps* and 150 *ps*, respectively. The maximum sampling frequency of Oscilloscope 12 is 1 GHz, given the use of a GHz type oscilloscope one can expect a time precision of at best 0.1 *ns*. This guarantees that the times of the incident laser signals and the AP spark signals can be distinguished.

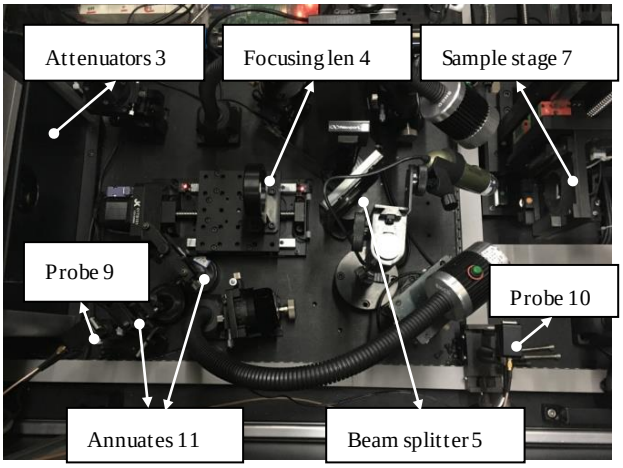

Fig. 3. Experiment configuration

All of experiments were done in a set of laser damage threshold test devices developed by our team. In this test device, the relative position of the laser, focusing system and the sample table have been fixed. Therefore, the focusing spot radius of the arrival sample platform will not change theoretically. In addition, pulse width of the laser is also fixed. Therefore, all measurements above were carried out only in function of the laser energy.

4. Experimental results and analysis

In all experiments, the incident laser signal is taken as the reference signal, and air plasma spark time (t_b) is the difference between the starting time of the air plasma flash signal and the reference signal. Therefore, in order to make the measurement results accurate and reliable, it is necessary to verify that the signal collected by Probe (9) is indeed the incident laser signal firstly. The whole experiment is carried out in the dark space. In order to avoid the signal interference, the incident laser energy is less than the energy required for the air to be broken down (about 150*mJ*), and the air plasma spark can not be produced, then the signal collected by the Probe (9) is the incident laser signal. In order to eliminate other disturbances, the connection line between Probe (10) and oscilloscope (12) is disconnected.

The incident laser signal obtained under different incident laser energy is shown in Fig. 4.

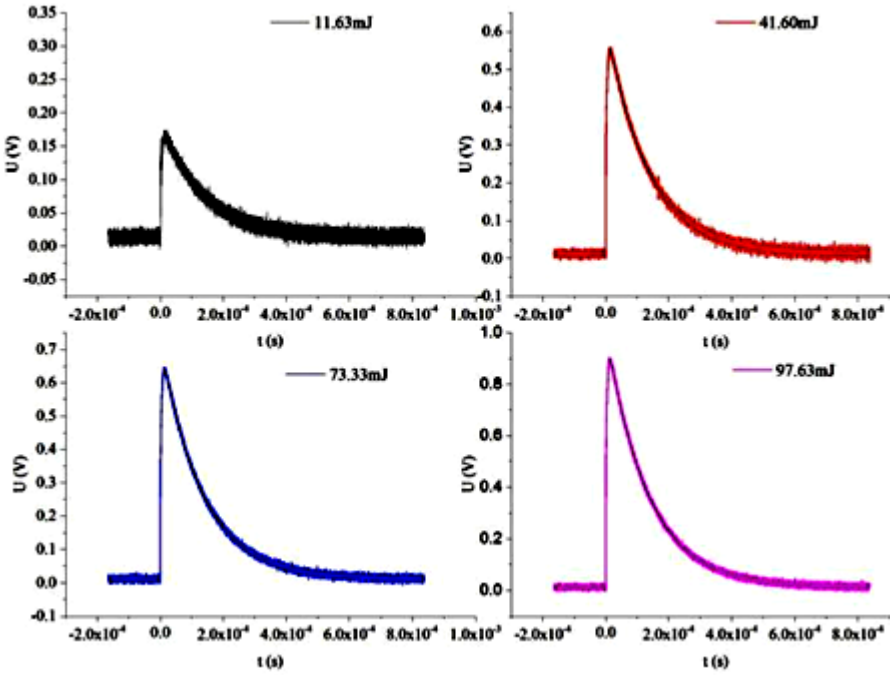

Fig. 4. The incident laser signal diagram

In Fig. 4, the energy of the incident laser energy is randomly chosen to be smaller than the energy required for the breakdown of the air. When the incident laser energy were 11.63*mJ*, 41.60 *mJ*, 73.33 *mJ* and 97.63 *mJ*, the peak values of the incident laser signals were about 0.15V, 0.58V, 0.64V, 0.90V. respectively. Fig. 4 shows that the peak values of the incident laser signal were increased with an increase in the incident laser energy. It indicated that the signal collected in the experiment was indeed the incident laser signal. When Probe (10) and oscilloscope (12) were connected, the following experimental results were obtained.

In Fig. 5(a), the energy of the incident laser was 228.38 *mJ*. Oscilloscope 12 collected the incident laser signals and the spark signals of AP produced during laser-induced breakdown over a sampling time of 200 *μs*. The figure shows that the amplitude step times of the incident laser and spark signals increased at 0 *ns* and then decreased to 0 V after several hundred millisecond. This process is consistent with that of pulsed light signals [10,23], suggesting that the sparks in this paper can be processed as pulse signals.

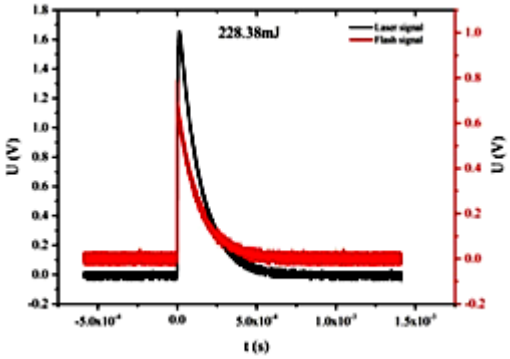

(a) Original Image

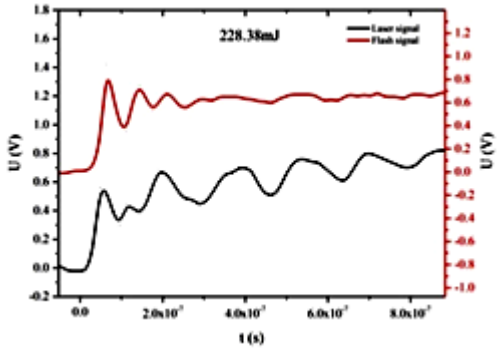

(b) Enlarged Image

Fig. 5. Signal diagram (Laser intensity = 228.38 mJ)

To obtain signal details, Fig. 5(a) was enlarged (Fig. 5b). The spark signals illustrated in Fig. 5(b) was fundamentally consistent with the spark signals of AP produced during the laser-induced breakdown proposed in a previous study [23]. The signals presented a number of continuous peak values, the main reason for this phenomenon is inverse bremsstrahlung process. Laser radiation is absorbed in the priming plasma by inverse bremsstrahlung, at the beginning of the inverse bremsstrahlung process, this absorption coefficient increases with the increase of electron density. Hence, the rate of absorption, and with it the rate of ionization escalates so that the electron density increases further and eventually approaches the critical density at which stage the critical density is established across a plane surface some distance into the plasma. At this surface the plasma becomes opaque to the incoming radiation which is therefore reflected outwards again. When the plasma becomes opaque laser radiation can no longer reach the surface of the target to generate new plasma by evaporation and ionization. Plasma growth however does not cease. Because of the heating which follows the absorption of energy by inverse bremsstrahlung, the plasma is driven rapidly away from the target surface; consequently the electron density decreases and the laser again reaches the target. These processes do not take place discontinuously however but merge into a smooth self-regulating regime with the generation, heating and expansion of plasma taking place throughout the length of the laser pulse.

In the experimental results, the increase of electron density is actually the increase of voltage. Therefore, there is an obvious attenuation for the peak values of the air plasma spark signals in a different time range. Subsequently, the sampling time of Oscilloscope 12 was reduced to enhance the accuracy of the measured times and obtain the signals during laser intensities of 230.59 *mJ*, 200 *mJ*, and 160 *mJ*, the signals of which are illustrated in Fig. 6, Fig. 7, and Fig. 8, respectively.

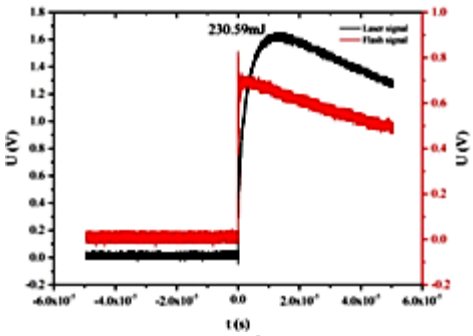

(a) Original image

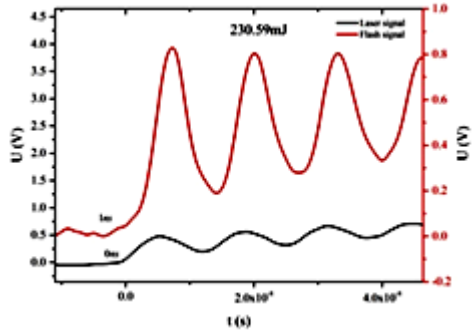

(b) Enlarged image

Fig. 6. Signal diagram (Laser intensity = 230.59 mJ)

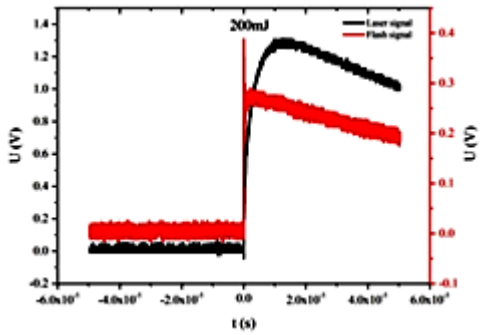

(a)Original Image

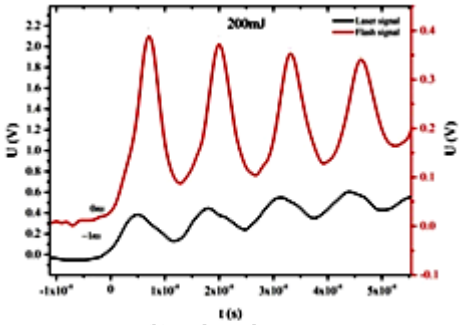

(b) Enlarged Image

Fig. 7. Signal Diagram (Laser Intensity = 200 mJ)

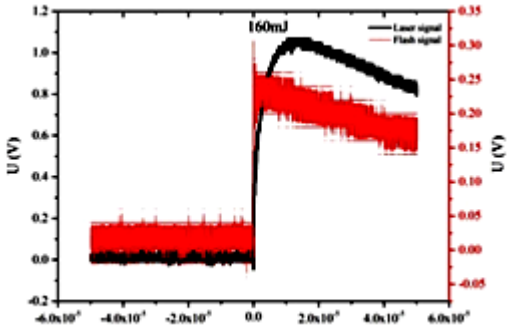

(a) Original Image

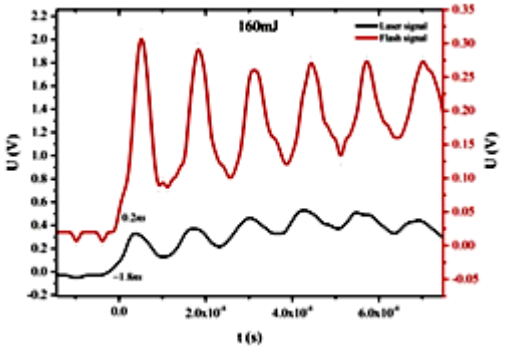

(b) Enlarged Image

Fig. 8. Signal Diagram (Laser intensity = 160 mJ)

Figs. 6(a), 7(a), and 8(a) are the original signal diagrams. The three figures show that the peak values of the incident laser signals decreased, respectively, to 1.63 V, 1.31 V, and 1.05 V and concurrently with laser intensity. The peak values of the AP spark signals also decreased respectively to 0.84 V, 0.404 V, and 0.32 V and concurrently with laser intensity, suggesting that AP sparks are closely associated with the incident laser intensity. Moreover, Fig. 6(a), Fig. 7(a), and Fig. 8(a) indicated obvious step peaks of the spark signals during the flash initialization stage. This was consistent with the findings of a previous study [23]. The flash initialization stage was analyzed to determine t_b. Therefore, Fig. 6(a), Fig. 7(a), and Fig. 8(a) were enlarged to produce Fig. 6(b), Fig. 7(b), and Fig. 8(b), respectively.

In Fig. 6(b), the incident laser and AP spark signals occurred at a positive value close to 0 *ns* and 1 *ns*, respectively. Therefore, $t_b \approx 1$ *ns*. In Fig. 7(b), the incident laser and AP spark signals occurred at −1 *ns* and a negative value close to 0 *ns*, respectively. Therefore, $t_b \approx 1$ *ns*. In Fig. 8(b), incident laser and AP spark signals occurred at −1.8 *ns* and 0.2 *ns*, respectively. Therefore, $t_b = 2$ *ns*. These results were consistent with the conclusion proposed in a previous study [10], which reported that AP ignites within a few nanoseconds. Figs. 6(b), 7(b), and 8(b) further show that the ST of AP reduced slightly as laser intensity increased. When all variables remain the same, a microanalysis revealed that the absorption of laser energy by air atoms or molecules near the focal point increased concurrently with an increase in laser intensity, accelerating the ionization of the atoms or molecules and the formation of high-temperature, high-density plasma. The plasma then absorbed the remaining laser energy and rapidly expanded to form AP sparks, which constitute a decrease in t_b.

In summary, the theoretical and experimental t_b under different laser intensities are tabulated in Table 1.

Table 1. Comparison of the theoretical and experimental t_b under different laser intensities

Incident laser intensity (*mJ*)	160	200	230.59
Theoretical t_b (*ns*)	2.146	1.595	1.854
Experimental t_b (*ns*)	2	1	1

Table 1 shows that the t_b values were 2.146 *ns*, 1.959 *ns*, and 1.854 *ns* at laser intensities of 160 *mJ*, 200 *mJ*, and 230.59 *mJ* respectively. The experimental t_b values were 2 *ns*, 1 *ns*, and 1 *ns* at laser intensities of 160 *mJ*, 200 *mJ*, and 230.59 *mJ* respectively. These results showed that the experimental values were similar to the theoretical values. The error margin might have been caused by the response times of the probes and the sampling frequency of the oscilloscope. Nonetheless, both the sets of simulation data confirmed that t_b reduces slightly as laser intensity increases.

5. Conclusions

Calculating t_b allows us to prevent film damage from misinterpreting. The resistance of the optical thin film to

laser affects commonly used laser-induced damage threshold (LIDT). Usually, the thin film has already been damaged if the thin film plasma spark occurs. However, the thin film plasma spark may be accompanied by an air plasma spark, if a spark is detected, which may be caused by air or thin film breakdown. In this case, to misinterpret film damage is possible. The spark can be distinguished according to the different ignition times. This can help us judge the damaged condition of the thin film accurately.

In this paper, a Nd:YAG nanosecond-pulse laser operating at 1064 nm was used to break down air. DET08CL/M and DET025AL/M, high-speed free-space detectors manufactured by THORLABS, were used to collect the incident laser and AP spark signals. The signals were displayed using the MSO2024B oscilloscope manufactured by Tektronix. The time differences between the occurrence of the incident laser and the AP spark signals were measured to determine the experimental t_b values. The MPA and CI theories were applied to simulate the theoretical t_b values. Results showed that when the laser pulse width was 10 *ns*, and the radius of the focal point of the incident laser was 0.015 *cm*, the experimental t_b values were 2 *ns*, 1 *ns*, and 1 *ns* at laser intensities of 160 *mJ*, 200 *mJ*, and 230.59 *mJ*, respectively. Under similar parameters, the theoretical t_b values were 2.146 *ns*, 1.959 *ns*, and 1.854 *ns* at laser intensities of 160 *mJ*, 200 *mJ*, and 230 59 *mJ*, respectively. Both the sets of data confirmed that t_b reduces slightly as laser intensity increases.

The findings obtained in this study not only revealed the mechanisms involved in the initial formation of AP during laser-induced breakdown but also provided a technical basis for detecting the plasma sparks of thin film damage.

Acknowledgements

This work was supported in part by Natural National Science Foundation of China (NSFC) (No. 61378050); International Science and Technology Cooperation Program of China (No. 2013DFR70620).

References

[1] M. Young, M. Hercher, Y. W. Chung, Journal of Applied Physics **37**(13), 4938 (1996).
[2] D. E. Lencioni, J. Appl. Phys. **48**(5), 1848 (1977).
[3] Zhengfang Song, China Meteorological Press, (1990).
[4] N. Kawahara, J. L. Beduneau, T. Nakayamal, Appl. Phys. B **86,** 605 (2007).
[5] Yanji Hong, Xing Jin, Qin Li, Zhiguo Du, Introduction to Getter Pulse Laser Propulsion, (National Defence Industry Press, 2012).
[6] Seong Y. Oh, Changhwan Lim, Sung Yong Ha, Sungmo Nam, Jaemin Han, Japanese Journal of Applied Physics **54**(7), 076101(2015).
[7] Junhong Su, Junqi Xu, Chen Yang, Surface Review and Letters **22**(6), 1550070 (2015).
[8] Chen Yang, Lingxia Hang, Junqi Xu, Materials Science in Semiconductor Processing **29**, 321 (2015).
[9] Su Junhong, Lv Ning, Ge Jinman, Chinese Journal of Lasers **43**(12), 1203003 (2016).
[10] C. Grey. Morganz, Rep. Prog. Phys. **38**, 623 (1975).
[11] Xueji Xu, Dingchang Zhu, Gas Discharge Physics, (Fudan University Press,1996).
[12] Jinji Xiang, Gas Discharge, (Science Press, 1983).
[13] P. E. Nielsen, G. H. Canavan, Journal of Applied Physics **44**(9), 4224 (1973).
[14] M. Young, M. Hercher, Journal of Applied Physics **38**(11), 4393 (1967).
[15] E. Sturmer, M. Allmen, Journal of Applied Physics **49**(11), 5648 (1978).
[16] Nan Zhang, Zehua Wu, Kuanhong Xu, Xiaonong Zhu, Optics Express **20**(3), 2528 (2012).
[17] Jiabin Zhu, Zhonggang Ji, Yunpei Deng, Jiansheng Liu, Ruxin Li, Zhizhan Xu, Optics Express **14**(11), 4915 (2006).
[18] Zhou Jun, Feng Liwei, Liu Yong, Xu Zhenhua, Journal of Applied Optics **32**(5), 1027 (2011).
[19] Liu Yu-Feng, Ding Yan-Jun, Peng Zhi-Min, Huang Yu, Du Yan-Jun, Acta Phys. Sin. **63**(20), 205205 (2014).
[20] Zefeng Yang, Wenfu Wei, Jiaxun Han, Jian Wu, Xingwen Li, Shenli Jia, Physics of Plasmas **22**(7), 073511 (2015).
[21] Sun Chengwei, Laser Irradiation Effect, National Defence Industry Press, (2002).
[22] Lu Jian, Ni Xiao-Wu, He An-Zhi, Physics of Interaction Between Laser and Materials, China Machine Press, (1996).
[23] Chen Lang, Lu Jianying, Wu Junying, Feng Changgen, Laser Supported Detonation Wave, National Defence Industry Press, (2011).
[24] Wang Guixia, Su Junhong, Xu Junqi, Yang Lihong, Wu Shengjiang, Acta Optica Sinica **37**(4), 0431001 (2017).

*Corresponding author: sujhong@126.com